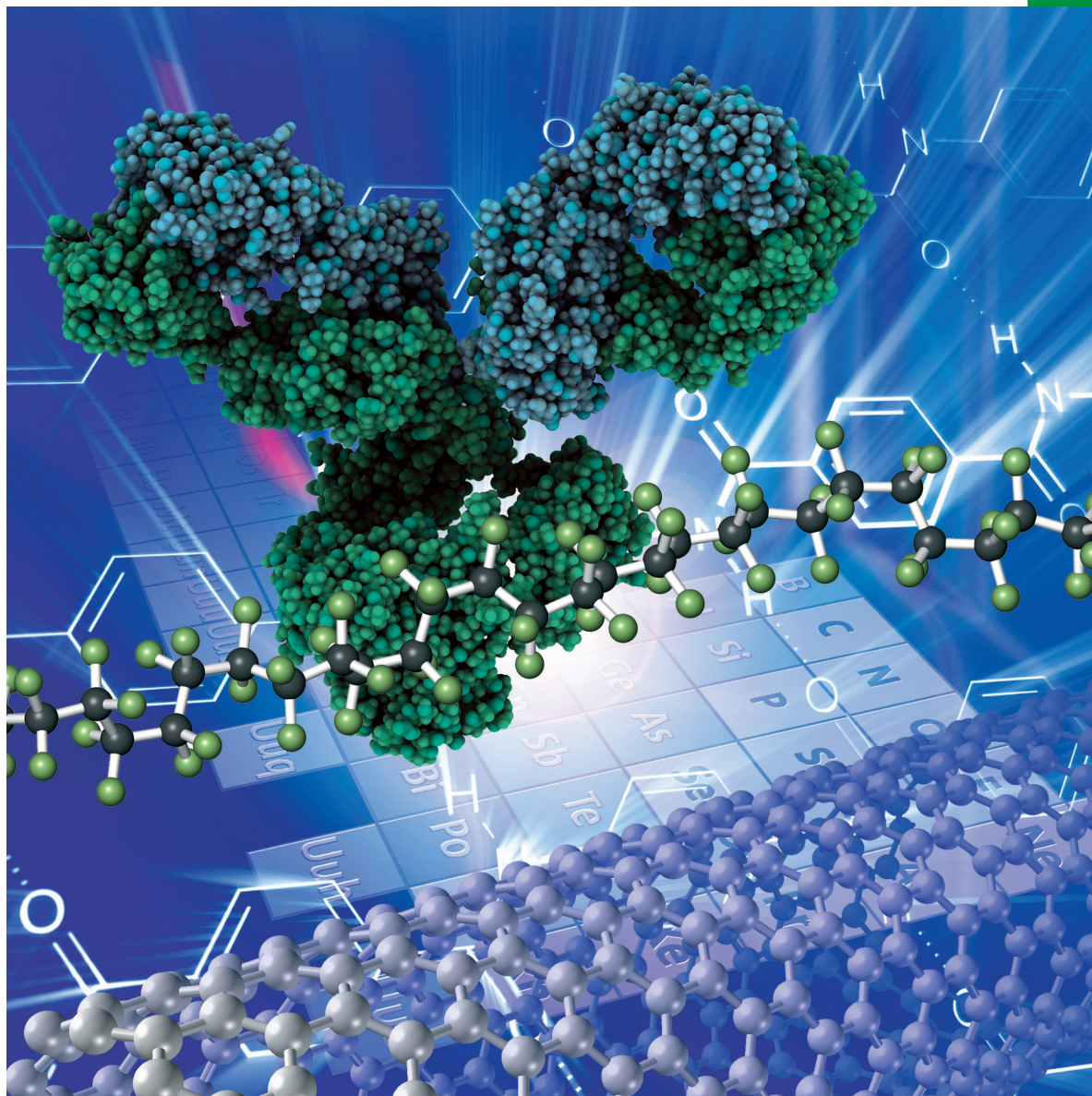


Chemistry **SELECT** ✓

www.chemistryselect.org

A journal of



REPRINT

WILEY-VCH

■ Catalysis

Ultrasound-Assisted Synthesis of Nitrogen and Oxygen Containing Heterocycles Using Fluorinated Graphene Oxide as Catalyst: Evaluation of Their Anthelmintic Activities

Arup Dutta,^[a] Bhusan Chhetri,^[c] Ridaphun Nongrum,^[b] George Kupar Kharmawlong,^[a] Arun K. Yadav,^[c] and Rishanlang Nongkhaw^{*[a]}

Spirooxindole derivatives have been efficiently synthesized via a three-component reaction consisting of isatin, malononitrile/pyrazole and various 1,3-diketones using Fluorinated Graphene Oxide (FGO) as a green and metal free carbocatalyst, under sonication. The main advantages of this synthetic approach lie in its operational simplicity, easy catalyst recovery and recyclability, high yields and short reaction times. The prepared catalyst was characterized by various analytical techniques viz., UV-Vis, FT-IR Spectroscopy, TGA, TEM, FE-SEM and EDX. The in vitro anthelmintic screening of synthesized compounds against a cestode, *Raillietina* sp. and a nematode parasite, *Syphacia*

obvelata at 200 µg/mL and 800 µg/mL were also carried out which revealed a profound activity, with much reduced mortality time of parasite. The SEM study indicated structure alterations in treated parasite, further validating the in vitro anthelmintic property. In addition, molecular docking studies were carried out against β-tubulin protein to determine binding affinity of the synthesized compounds. All test compound followed the "Lipinski Rule of Five" and in silico pharmacokinetic investigation showed inhibitory activity against CYP enzyme and P-glycoprotein which may further improve the bio efficacy of compounds.

1. Introduction

Graphene-based nanomaterials have gained a wide spread attention due to their unique electrical and mechanical properties. These materials have found applications in many fields, such as photocatalysts,^[1] bio-sensors,^[2] supercapacitors,^[3] etc. Further, chemical modification of Graphene Oxide have simulated interest amongst synthetic and theoretical chemists due to its enhanced and excellent electronic properties. Fluorination has been found to be one of the strategies adopted for the covalent functionalization of graphene since Fluorine has high reactivity with respect to catalytic properties and behaves as an insulator due to its high band gap.^[4] Also being the most electronegative element in the Periodic Table, Fluorine has made FGO to exhibit excellent oxidative and catalytic properties.^[5] Therefore, the exploration of customized graphene-based catalyst is highly significant.

Nitrogen and oxygen containing spirooxindoles are a privileged class of compounds having great relevance in biological and medicinal fields such as vasodilators,^[6] antitumor,^[7] antidiabetic,^[8] antipyretic,^[9] and analgesic,^[10] etc. Due to their extensive importance in biological system, various methodologies have been developed for their synthesis.^[11 (A-J)] Spirooxindole derivatives have also been synthesized using a variety of catalysts, such as TiCl₄,^[12A,B] L-proline,^[13] MnFe₂O₄,^[14] Et₃N,^[15] ZnFe₂O₄,^[16] Fe₃O₄@GO@SO₃H,^[17] etc.

Lately, ultrasonication has been used for many bond formation reactions such as C–C,^[18] C–N,^[19] and C–O bond.^[20] The efficiency of this technique to disperse the reaction particles^[21] has not only reduced the reaction time but has also improved the yield of the products.^[22]

Helminthias has been found to be a serious health problem worldwide and it is amongst the most common infections affecting mostly the low-income and resource-poor populations.^[23] Helminth infections increases the disability-adjusted life year (DALYs) of vulnerable individuals and also immensely affects the productivity of livestock.^[24] It has been much advocated that in coming decades, with climate change, population explosion and migration,^[25] incidence of helminth infection will rise rapidly.^[26] Even a worst scenario could happen in future with dependence only on limited drugs and escalating cases of resistant helminth strains against drug candidates.^[27]


A broad spectrum of biological activities of spirooxindole derivatives, as mentioned earlier, prompted us to investigate their anthelmintic properties.

In continuation with our endeavour towards environmental benign protocols, we report herein a metal-free recyclable FGO

[a] A. Dutta, G. Kupar Kharmawlong, Dr. R. Nongkhaw
Department of Chemistry
North-Eastern Hill University, Shillong
Meghalaya-793022 (India)
E-mail: rlnongkhaw@gmail.com

[b] Dr. R. Nongrum
Department of Chemistry
Sankardev College, Shillong
Meghalaya-793004 (India)

[c] B. Chhetri, Prof. A. K. Yadav
Department of Zoology
North-Eastern Hill University, Shillong
Meghalaya-793022 (India) Institution

 Supporting information for this article is available on the WWW under <https://doi.org/10.1002/slct.202001442>

carbocatalyst for the synthesis of spirooxindole derivatives under ultrasonic conditions. The synthesized compounds were further evaluated for their anthelmintic activities.

2. Results and Discussion

We have developed an efficient and economical method for the synthesis of spiro derivatives of oxygen and nitrogen heterocycles *via* a three-component reaction consisting of isatin, malononitrile/ pyrazole and various 1,3-diketones under ultrasonic condition by employing FGO as a green catalyst in water.

2.1. Catalyst fabrication and characterization

Graphite oxide (GO) was prepared by the modification of Hummers's method from natural graphite powder.^[28] Fluorinated graphene oxide (FGO) was obtained through a hydrothermal treatment of GO with nitric acid and hydrofluoric acid.^[29] The prepared catalyst was characterized using different techniques *viz.*, FT-IR, TGA, TEM, FE-SEM, EDX and UV-Vis spectroscopy.

2.2. Fourier transform infrared (FT-IR) spectroscopy

FT-IR spectra of (A) GO (B) FGO are shown in Figure 2. In A, the broad and strong band of around 3442 cm^{-1} can be assigned to the O–H stretching vibration while band at 1628 cm^{-1} can be attributed to C=C stretching vibration. The band at 1146 cm^{-1} corresponds to the C–O stretching vibration. In case of B, the equivalent band due to O–H stretching vibration

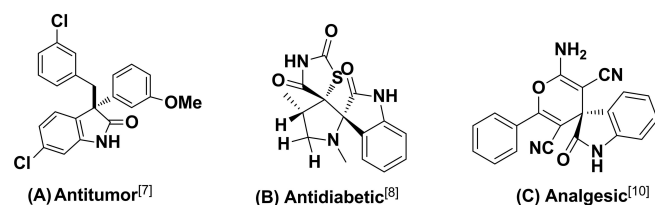


Figure 1. Some examples of medicinally active spirooxindoles (A–C).

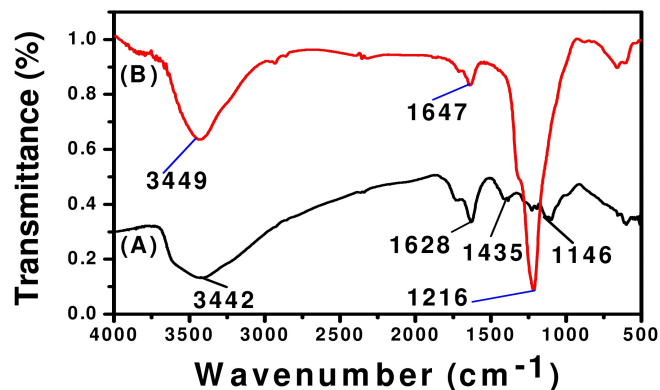


Figure 2. FT-IR spectra of: (a) GO (b) FGO.

appeared at 3449 cm^{-1} while the C=C stretching vibration appeared at 1647 cm^{-1} . The strong absorption peak at 1216 cm^{-1} can be assigned to the C–F stretching vibration which is absent in case of GO.

2.3. Thermogravimetric analysis (TGA)

TGA was performed to evaluate the thermal stability of the prepared FGO. As shown in Figure 3, a weight loss at about 100°C is attributed to the liberation of the intercalated water molecules on GO sheets. The major weight loss can be accounted of fluorinated graphene oxide in the temperature range of 450°C which constitutes about 85% of the total weight.

2.4. Field Emission Scanning electron microscopy (FE-SEM)

The morphology of the synthesized catalyst was determined by FE-SEM. Figure 4 indicates that the surface of FGO are irregular with overlapping steps and some of graphitic panes appeared to be curled up. Elemental mapping of FGO (Figure 5) indicated the homogeneous dispersion of the three elements *i.e.* C, O and F.

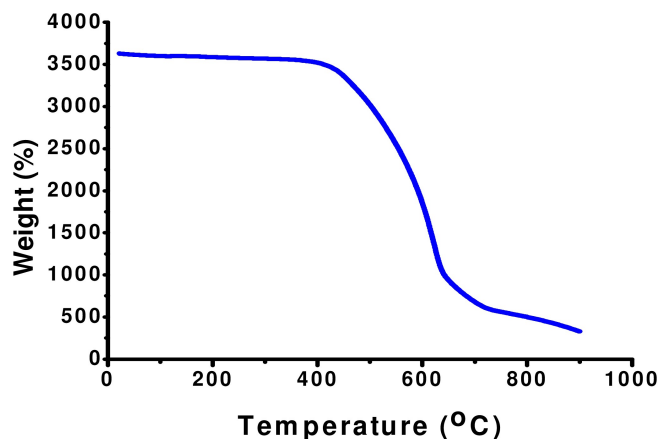


Figure 3. TGA spectrum of FGO.

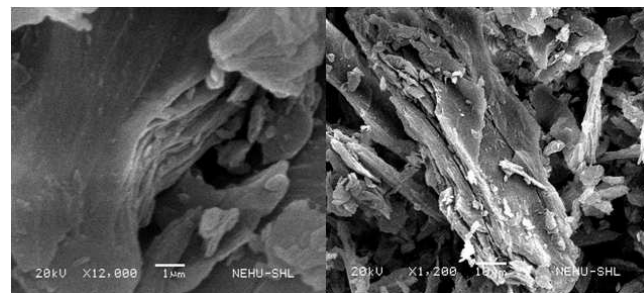


Figure 4. FE-SEM images of FGO.



Figure 5. Element mapping of FGO.

2.5. Transmission electron microscopy (TEM)

TEM was performed to investigate the microstructure quality of the prepared catalyst (Figure 6). The low magnification TEM images shows transparent wrinkles (Figure 6b) indicating the thinness of the sheet of FGO. High-resolution TEM image

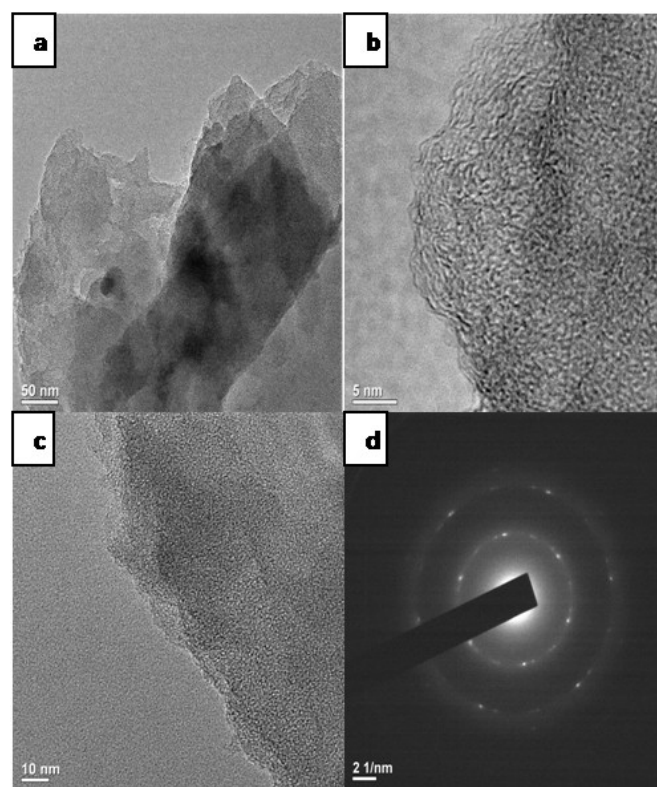


Figure 6. (a) Low resolution TEM, (b) & (c) High resolution TEM, (d) SAED pattern of FGO.

(Figure 6c) shows few lines along the boundary of the fluorinated graphene. SAED pattern (Figure 6d) reveals that FGO have high crystal quality with the appearance of a well-defined six-fold-symmetry pattern.

2.6. Energy Dispersive X-ray analysis (EDX)

The distribution of the elements was further studied by EDX (Figure 7) which showed the presence of carbon, oxygen and fluorine thus confirming the functionalization of fluorine to the GO sheets. The amount of the incorporated fluorine was determined and its percentage varied depending on the layers of the FGO.

2.7. UV-Visible Spectroscopy (UV-Vis)

The absorption spectra of GO and FGO were recorded, and the results are shown in Figure 8. The characteristic absorption maximum at around 270 nm region corresponds to the π - π^* and n - π^* transitions of C=C and carbonyl groups. After

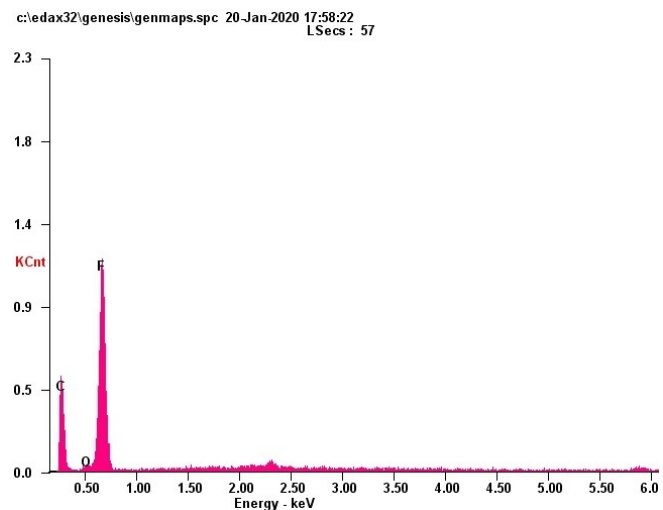


Figure 7. EDX peaks of FGO.

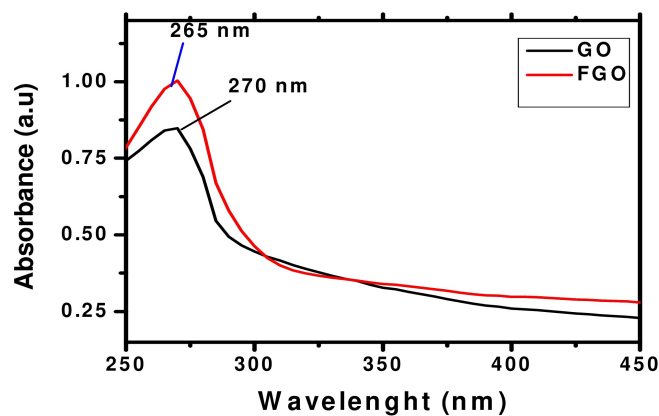


Figure 8. UV-Vis spectrum of GO and FGO.

fluorination, the absorption maximum appeared around 265 nm which may be due to the potential loss of the π -electron density.

2.8. Standardization of the reaction conditions

A reaction mixture consisting of isatin, malononitrile/pyrazole and 1,3-diketone was ultrasonicated in the presence of FGO as catalyst. As shown in Table 1, the different products were obtained in high to excellent yields, within a short reaction

Table 1. Synthesis of compounds 4 a–d, 5 a–f, 6 a, 7 a, 8 a–b, 9 a–b, 10 a–b and 11 a–e.							
Entry	R	Malononitrile/Pyrazole	1,3-diketone	Product	Ultrasonic condition Time (min)	Yield ^[a] (%)	Microwave condition Yield ^[b] (%)
1	H	2a	3a	4a	10	96	70
2	CH ₃	2a	3a	4b	15	92	68
3	NO ₂	2a	3a	4c	15	94	67
4	OCH ₃	2a	3a	4d	18	89	65
5	H	2a	3b	5a	10	87	61
6	CH ₃	2a	3b	5b	10	88	63
7	NO ₂	2a	3b	5c	15	90	69
8	Br	2a	3b	5d	18	87	66
9	OCH ₃	2a	3b	5e	15	86	61
10	Cl	2a	3b	5f	10	89	70
11	H	2a	3c	6a	10	96	72
12	H	2a	3d	7a	10	92	67
13	H	2a	3e	8a	10	90	69
14	NO ₂	2a	3e	8b	15	91	63
15	H	2b	3a	9a	15	93	71
16	Cl	2b	3a	9b	15	92	65
17	H	2b	3e	10a	15	89	68
18	NO ₂	2b	3e	10b	18	87	66
19	H	2c	3c	11a	18	93	71
20	CH ₃	2c	3c	11b	15	91	73
21	Cl	2c	3c	11c	15	90	69
22	OCH ₃	2c	3c	11d	20	88	67
23	Br	2c	3c	11e	18	91	69

[a] & [b] isolated yield

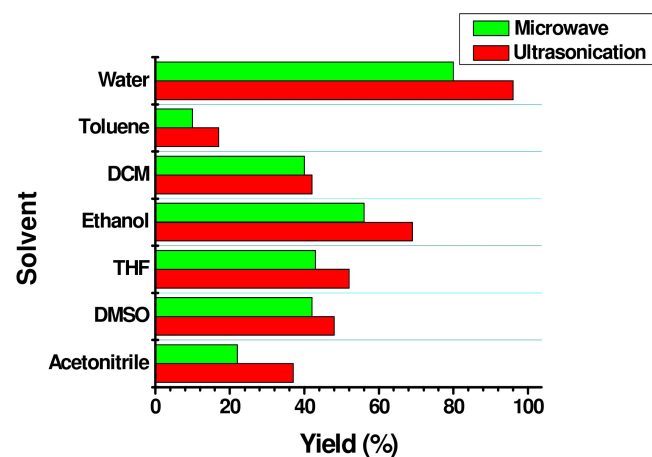


Figure 9. Optimization of the solvent for the synthesis of 6a.

time. All products were characterized using physical and spectroscopic techniques.

The efficacy of the catalyst in different media for a model reaction 6a was evaluated and the results are presented in Figure 9. It was observed that the reaction proceeded well in both polar and non polar solvents like N,N dimethylformamide, tetrahydrofuran, toluene, chloroform, ethanol and acetonitrile. However the yields were not satisfactory. The best yield was obtained when water was used as a solvent.

Studies were also done to investigate the optimum amount of catalyst required for the model reaction 6a and 15 mg was found to be the ideal amount (Figure 10).

On completion of the reaction, the catalyst was recovered from the reaction mixture by filtration and it was reused after washing with water and acetone. Owing to the heterogeneous property of the catalyst, its separation was easy and efficient (> 96%). The reusability of the prepared FGO was also studied and it was observed that there was no significant change in the yield of the product even after six cycles (Figure 11).

A comparative study of catalytic activity of the prepared FGO for the model reaction 6a at different conditions is presented in Table 2. As expected, because of the increased

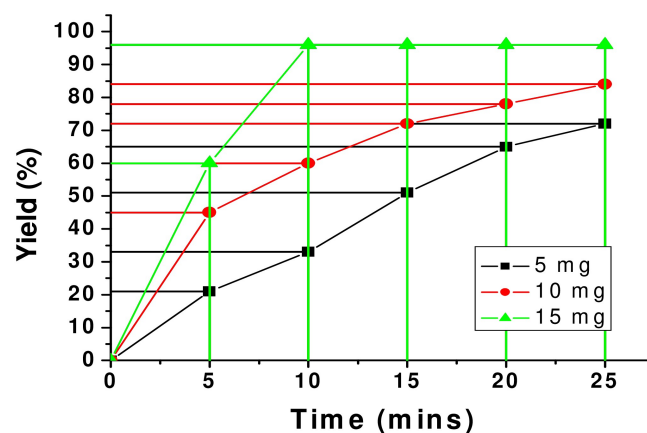


Figure 10. Optimization of catalyst loading for the synthesis of 6a.

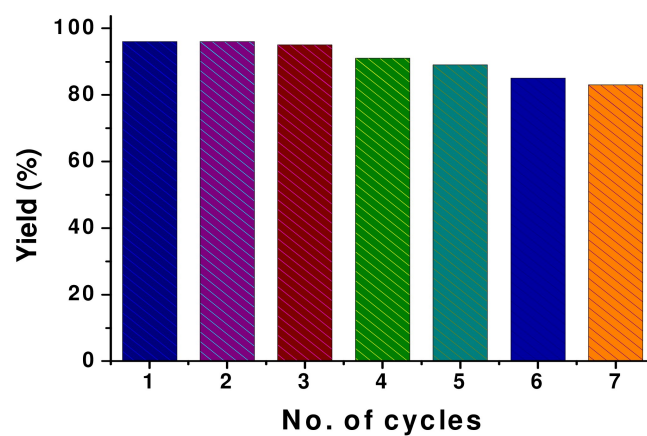


Figure 11. Recyclability plot of the catalyst for synthesis of 6a.

Table 2. Effect of catalysts and solvent on preparation of **6a**.

Catalyst	Condition	Solvent	Time (min)	Yield* (%)
No catalyst	Reflux	H ₂ O	15	15
No catalyst	Ultrasound	H ₂ O	15	20
No catalyst	Microwave	H ₂ O	15	10
GO	Ultrasound	H ₂ O : CH ₃ OH	15	70
GO	Microwave	H ₂ O	15	65
GO	Reflux	H ₂ O	15	68
GO	Room Temperature	H ₂ O	15	29
FGO	Reflux	H ₂ O	15	80
FGO	Microwave	H ₂ O	15	80
FGO	Ultrasound	H ₂ O	15	96
FGO	Ultrasound	H ₂ O	10	96

Reaction condition : Isatin (1 mmol), malononitrile (1 mmol), barbituric acid (1 mmol) in 10 ml of solvent, under ultrasonication (90%) and 50 °C, [*] Isolated yield

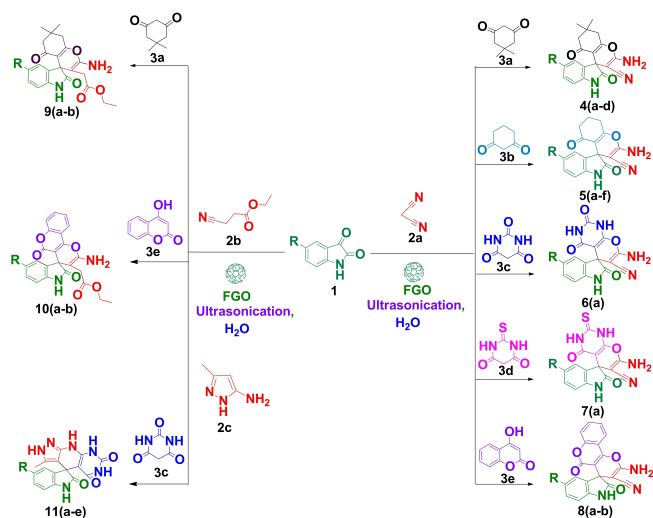
activity due to the presence of Fluorine atoms, FGO gave better yields as compared to GO. It was also observed that the reaction was completed in a shorter time under ultrasonication using water as solvent.

Under the optimized condition of catalyst and solvent, we further examined the effects of the ultrasonic probe power (%)

Table 3. Effects of the ultrasonic probe power on the formation of **6a**

Entry	Power (%)	Time (min)	Yield (%)*
1	30	15	55
2	40	15	60
3	60	15	75
4	80	15	85
5	90	15	96
6	90	10	96

Reaction condition : Isatin (1 mmol), malononitrile (1 mmol), barbituric acid (1 mmol) in 10 ml of solvent, under ultrasonication (90%) and 50 °C, [*] Isolated yield



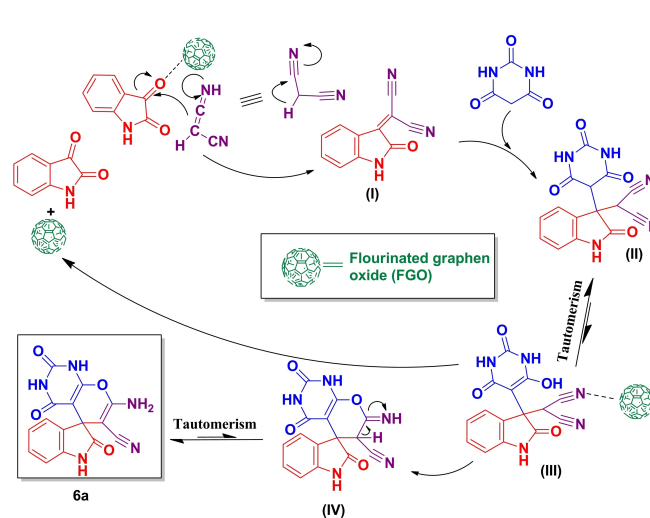
Scheme 1. Preparation of nitrogen and oxygen containing spiro compounds using FGO in water under ultrasonic condition.

on the yield of the product. From the results obtained, as depicted in Table 3, the most suitable ultrasonic power was 90% at 50 °C.

The plausible mechanistic pathway for the formation of 7'-amino-2,2',4'-trioxo-1',2',3',4'-tetrahydrospiro [indoline-3,5'-pyrano[2,3-d]pyrimidine]-6'-carbonitrile (**6a**) from isatin, malononitrile and barbituric acid is shown in Scheme 2. The catalyst coordinates with electrophilic carbonyl oxygen of isatin, which facilitates the nucleophilic attack of isatin by malononitrile leading to the formation of Knoevenagel condensation intermediate (I). This is followed by the Michael reaction with the cyclic 1,3-dicarbonyl compound to give (II). Finally, (II) undergoes cyclization followed by tautomerization to give the desired product **6a**.

2.9. Evaluation of anthelmintic studies

In vitro screening of the spirooxindole derivatives showed a reduction in mortality time for both *Syphacia* and *Rallietina* parasites, compared to worm's mortality in control medium at 55.88 ± 0.61 hr and 44.10 ± 0.861 hr, respectively (**Figure S13, supplementary Information**). Compound **5a**, **6a**, **7a** and **8a** at 800 $\mu\text{g/mL}$ concentration, showed higher anthelmintic efficacy, with worms mortality at 2.88 ± 0.129 hr, 2.83 ± 0.105 hr, 4.82 ± 0.154 hr and 4.18 ± 0.105 hr, respectively against *S. obvelata*, and at 1.74 ± 0.080 hr, 1.84 ± 0.113 hr, 2.40 ± 0.107 hr and 2.26 ± 0.093 hr, respectively against *Raillietina* sp. as compared to albendazole at 16.56 ± 0.186 hr and praziquantel at 6.51 ± 0.243 hr respectively. Further, at 200 $\mu\text{g/mL}$, the mortality time of parasites reduced significantly with respect to both the test parasites against the compound **5a**, which appeared to be the most potent derivative. Although, **5a** derivatives, that were substituted with $-\text{CH}_3$ (**5b**), $-\text{NO}_2$ (**5c**), $-\text{Br}$ (**5d**), $-\text{OCH}_3$ (**5e**), $-\text{Cl}$ (**5f**) displayed a comparatively reduced activity against both the helminths models, in the following order : $\text{NO}_2 > \text{CH}_3 > \text{Br} > \text{OCH}_3 > \text{Cl}$. Interestingly, the compound **4a** and its derivatives showed a biased activity, wherein compound **4a**,



Scheme 2. Plausible mechanism for the synthesis of **6a** using FGO as catalyst.

with $-\text{NO}_2$ as a substituent (**4c**), revealed a better efficacy against *Railletina* sp. with mortality at 4.44 ± 0.139 hr and 5.54 ± 0.106 hr. On the other hand, $-\text{CH}_3$ (**4b**) and $-\text{OCH}_3$ (**4d**) substitution showed mortality of *S. Obvelata* at 8.49 ± 0.087 hr and 9.48 ± 0.102 hr, at $800 \mu\text{g/mL}$. Compound **9a** and **10a** revealed the highest efficacy at $800 \mu\text{g/mL}$, with mortality of cestode at 6.02 ± 0.108 hr, 4.93 ± 0.131 hr and that of nematode at 17.52 ± 0.135 hr and 15.0 ± 0.134 hr, respectively. The overall results clearly dictates dose dependence in both the parasite model for all test derivatives. Electron donating and withdrawing group appears to play a vital role in determining the biological activity.

Structure-analysis relationship for the active compound **5a**, **6a**, **7a** and **8a** reveals potential anthelmintic efficacy which might be due to the presence of strong activating group. While, compound series **4a** show an increase in nematocidal activity with substituted electron donating ($-\text{CH}_3$ and $-\text{OCH}_3$) group, whereas better cestocidal activity was recorded with electron withdrawing ($-\text{NO}_2$) groups. Further, the substitution of **5a** with electron donating ($-\text{CH}_3$ and $-\text{OCH}_3$) and electron withdrawing ($-\text{NO}_2$, $-\text{Cl}$ and $-\text{Br}$) groups resulted in a substantial reduction in its activity.

The SEM observations of control cestodes revealed a smooth appearance of tegument, with an anterior-most scolex possessing regular rows of short and thick pointed hooklets (Figure 12. **A** and **E**). Likewise, the nematodes from control group revealed a normal morphology of surface cuticle, with regular transverse striations, and prominent lips in anterior region (Figure 12. **I** and **M**). On the other hand, the cestode parasites exposed to test compounds revealed a shrinkage, blebbing and erosion of tegument, which was accompanied with numerous distortions and a shrunken scolex (Figure 12. **B**, **C**, **F** and **G**). Similarly, *S. obvelata* worms exposed to derivatives showed a distorted surface cuticle, with lips appearing as clubbed together (Figure 12. **J**, **K**, **N** and **O**). Exposure of parasites to reference drugs, praziquantal and albendazole, also revealed an altered morphology of parasite body (Figure 12. **D**, **H**, **L** and **Q**). It is assumed that the hyper-contraction, paralysis and mortality of parasites occurred as a result of a combination of effects on the nervous system and helminth musculature. The observed effects of compounds on body surface of exposed parasites suggest a promising anthelmintic efficacy of tested spirooxindole derivatives.

The physicochemical properties (Table S4, Supplementary Information) predict that all the studied derivatives follow the "Lipinski rule of five", along with Total Polar Surface Area (TPSA) < 140 , considered ideal for better bioavailability. The pharmacokinetics studies (Table S5, Supplementary Information) of test derivatives reveal a high gastro-intestinal absorption. However, it appeared that the blood brain barriers cannot be crossed herein. Most compounds inhibited the isoforms of Cytochrome P450 (CYP) family, such as CYP1 A2 and CYP2 C9, allowing minimizing the first pass metabolism. It may be noted herein that the compounds interacting with P-glycoprotein as substrate normally leads to a higher bioavailability. The results also showed that compounds **6a** and **7a** possess a significant in vitro efficacy, though with a higher TPSA and low logP value,

and the gastro-intestinal absorption and bioavailability was also noted to be reduced dramatically. Spirooxindole derivatives inhibiting CYP enzyme and P-glycoprotein may lead to higher concentration in blood circulation thus enhancing activity. Anthelmintics used solely to treat gastrointestinal infestations do not need to be absorbed to be effective and their pharmacological action probably relates to that fraction which is not absorbed these can be a possible explanation for activity of **6a** and **7a**.

Molecular docking study (Figure S14, Supplementary Information) reveals binding energy for spirooxindole derivatives within -10.0 and -6.4 Kcal/mol, indicating strong affinity for the target. The binding energy was almost similar, for the compound of **5a**, **6a**, **7a** and **8a** though the hydrogen bonds showing one, three, six and ten, respectively. Compound **5a** formed only one hydrogen bond with Arg318. On the other hand, compound **6a** formed one hydrogen bond with residues Arg318 and two hydrogen bonds with Gln43. Moreover, compound **7a** formed one hydrogen bond with residues Gln11, Thr143, Thr178, Asp177 and two hydrogen bonds with Ser138. Whereas, compound **8a** formed one hydrogen bond with each residue Gln11, Asn99, Gly142, Thr178, Ser138, three hydrogen's bond with Thr143 and two hydrogen bonds with Gly144. Albendazole show binding energy of -6.4 with only one hydrogen bond with Ala 283. The binding affinity of spirooxindole with β -tubulin proteins is crucial for anthelmintic development. Helminth survival depends on interacting microtubules for mitosis, motility, and transport, disrupting any of these vital functions may into paralysis and mortality. Hydrogen bond formation result in stabilizing of interacting residue with the target protein, higher the number of hydrogen bond stronger the interaction. Binding energy less than -6.0 kcal/mol for a ligand-protein interaction will reflect its activity. Moreover, characterization of binding interactions shows that compound **7a** and **8a** form more intermolecular interactions composed of hydrogen with β -tubulin which may lead to better anthelmintics.

3. Conclusion

Here, we have developed an environmentally friendly, non-toxic, highly efficient, stable and recyclable FGO as a catalyst for the synthesis of C–N and C–O bond heterocycles in aqueous medium under ultrasonic condition. In addition, the catalytic methodology offers advantages, such as high yields, low catalyst requirement, short reaction times, usage of green solvent, column free work up condition and easy catalyst recyclability. Furthermore, the biological importance of the prepared spirooxindole derivatives shows high anthelmintic activities. The observation can further be explored to investigate in vitro studies in the near future. Based on our findings drug-parasite interaction are likely to affect parasite motility and vitality through disruption in surface topography. Interestingly, most active compounds show far better anthelmintic efficacy than positive control against both the cestode and nematode parasite. The binding energy and hydrogen bonds results obtained from molecular docking study validates in vitro

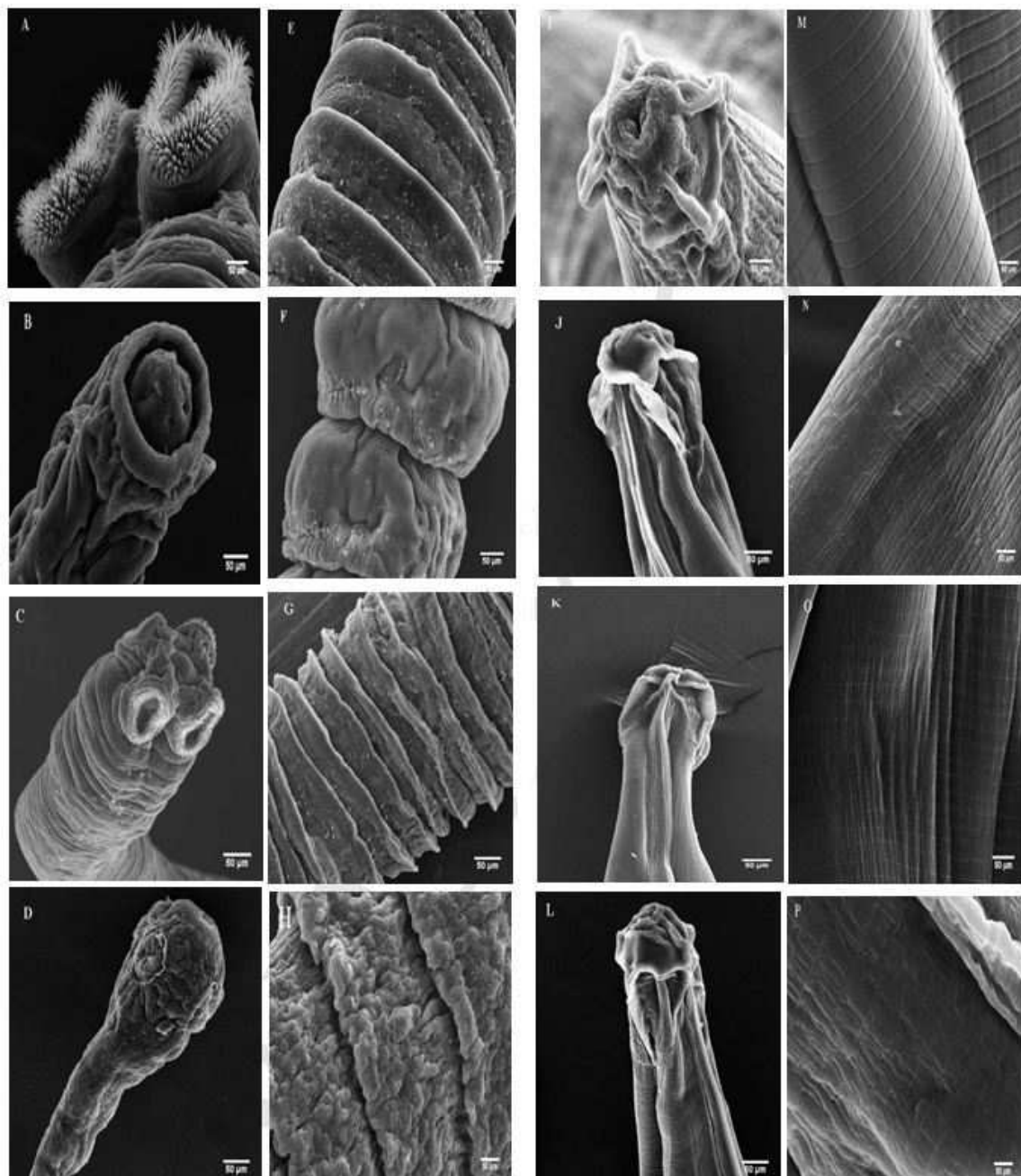


Figure 12. SEM images of mature *Raillietina* sp. scolex (A–D) and segment (E–H); *Syphaciaobvelata* cephalic region (I–L) and Cuticle (M–P); Negative control (A,E,I,M); Positive control (D,H,L,P); Treated 5a (B,F,J,N) and Treated 6a (C,G,K,O) at 800 µg/mL.

anthelmintic activity. Despite some limitations to *in silico* methodology, it does provide valuable insight to drug likeness of spirooxindole derivatives. Further investigation of compound on *in vivo* model and also toxicity studies may assist in designing of novel anthelmintics.

Supplementary Information Summary

The experimental details, the spectral data along with the spectra can be found in the Supplementary Information Section.

Acknowledgements

The author would like to acknowledge the Department of Chemistry-NEHU, SAIF-NEHU, IIT-Madras and for providing various facilities in carrying out the present work is highly acknowledged.

We would like to thank DST for financial support (sanctioned no.: EEQ/2016/000646). The support and encouragement received from the Dr. Davendra Biswal, Centre for Bioinformatics, NEHU, Shillong is gratefully acknowledged.

Conflict of Interest

The authors declare no conflict of interest.

Keywords: Anthelmintic Activities · Fluorinated Graphene Oxide Heterocycles · Molecular docking · Spirooxindole

- [1] J. Low, J. Yu, W. Ho, *J. Phys. Chem. Lett.* **2015**, *6*, 4244–4251.
- [2] R. Zhang, W. Chen, *Biosens. Bioelectron.* **2017**, *89*, 249–268.
- [3] Z. Yang, J. Tian, Z. Yin, C. Cui, W. Qian, F. Wei, *Carbon.* **2019**, *141*, 467–480.
- [4] M. Pumera, Z. Sofer, *Chem. Soc. Rev.* **2017**, *46*, 4450–4463.
- [5] M. G. Campbell, T. Ritter, *Chem. Rev.* **2015**, *115*, 612–633.
- [6] M. Borcosque, F. E. C. Jorquera, B2, US 9, 663453, **2017**.
- [7] D. Katayev, E. P. Kundig, *Helvetica. Chimica. Acta.* **2012**, *95*, 2287–2295.
- [8] R. Murugan, S. Anbazhagan, S. S. Narayanan, *Eur. J. Med. Chem.* **2009**, *44*, 3272–3279.
- [9] D. do Carmo Malvar, R. T. Ferreira, R. Andrade de Castro, L. L. de Castro, A. C. C. Freitas, E. A. Costa, I. F. Florentino, J. C. M. Mafra, G. E. P. ouza, F. A. Vanderlinde, *Life Sci.* **2014**, *95*, 81–88.
- [10] Y. Sun, J. Liu, X. Jiang, T. Sun, L. Liu, X. Zhang, S. Ding, J. Li, Y. Zhuang, Y. Wang, R. Wang, *Sci. Rep.* **2015**, *5*, 1–7.
- [11] a) V. Rathore, S. Kumar, *Green Chem.* **2019**, *21*, 2670–2676. b) Z. Y. Cao, F. Zhou, J. Zhou, *Acc. Chem. Res.* **2018**, *51*, 1443–1454. c) P. B. Alper, C. Meyers, A. Lerchner, D. R. Siegel, E. M. Carreira, Facile, *Angew. Chem. Int. Ed.* **1999**, *38*, 3186–3189. d) K. Shen, X. Liu, L. Lin, X. Feng, *Chem. Sci.* **2012**, *3*, 327–334. e) S. Kumar, V. Rathore, A. Verma, C. D. Prasad, A. Kumar, A. Yadav, S. Jana, M. Sattar, Meenakshi, S. Kumar, *Org. Lett.* **2015**, *17*, 82–85. f) T. Shen, Y. Yuana, N. Jiao, *Chem. Commun.* **2014**, *50*, 554–556. g) C. D. Prasad, M. Sattar, S. Kumar, *Org. Lett.* **2017**, *19*, 774–777. h) T. L. Pavlovska, R. G. Redkin, V. V. Lipson, D. V. Atamanuk, *Mol. Divers.* **2016**, *20*, 299–344. i) M. Sattar, V. Rathore, C. D. Prasad, S. Kumar, *Chem. Asian J.* **2017**, *12*, 734–743. j) G. Bhaskar, Y. Arun, C. Balachandran, C. Saikumar, P. T. Perumal, *Eur. J. Med. Chem.* **2012**, *51*, 79–91.
- [12] a) G. Abbiati, A. Casoni, V. Canevari, D. Nava, E. Rossi, *Org. Lett.* **2006**, *8*, 4839–4842. b) J. J. Badillo, G. E. Arevalo, J. C. Fettinger, A. K. Franz, *Org. Lett.* **2010**, *13*, 418–421.
- [13] Y. Li, H. Chen, C. Shi, D. Shi, S. Ji, *J. Comb. Chem.* **2010**, *12*, 231–237.
- [14] R. Ghahremanzadeh, Z. Rashid, A. H. Zarnani, H. Naeimi, *Appl. Catal. A-Gen.* **2013**, *367*, 270–278.
- [15] B. Zhou, Z. Luo, Y. Li, *Chem. Eur. J.* **2013**, *19*, 4428–4431.
- [16] H. Hasani, M. Irizeh, *Asian J. Green Chem.* **2018**, *2*, 85–95.
- [17] M. Abdi, S. Rostamizadeh, N. Zekri, *Polycycl. Aromat. Comp.* **2017**, *39*, 413–424.
- [18] G. Brahmachari, *RSC Adv.* **2016**, *6*, 64676–64725.
- [19] Y. Wu, Z. Chen, W. C. Cheong, C. Zhang, L. Zheng, W. Yan, R. Yu, C. Chen, Y. Lia, *Chem. Sci.* **2019**, *10*, 5345–5352.
- [20] S. N. Maddila, S. Maddila, M. Khumalo, S. V. H. S. Bhaskaruni, S. B. Jonnalagadda, *J. Mol. Struct.* **2019**, *1185*, 357–360.
- [21] P. Moilanen, A. Salmi, V. Kilappa, Z. Zhao, J. Timonen, E. Haeggström, *J. Appl. Phys.* **2017**, *122*, 144901–144906.
- [22] R. Sivaramakrishnan, A. Incharoensakdi, *Fuel.* **2017**, *191*, 363–370.
- [23] P. J. Hotez, P. J. Brindley, J. M. Bethony, C. H. King, E. J. Pearce, J. Jacobson, *J. Clin. Invest.* **2008**, *118*, 1311–1321.
- [24] M. P. Murtaugh, C. J. Steer, S. Sreevatsan, N. Patterson, S. Kennedy, P. Sriramarao, *Ann. N. Y. Acad. Sci.* **2017**, *1395*, 12–32.
- [25] A. J. Blum, P. J. Hotez, *PLoS Negl. Trop. Dis.* **2018**, *12*, 1–6.
- [26] J. E. Truscott, J. C. Dunn, M. Papaikovou, F. Schaer, M. Werkman, D. T. J. Littlewood, J. L. Walson, R. M. Anderson, *PLoS Negl. Trop. Dis.* **2019**, *13*, 1–14.
- [27] E. J. Lenk, W. K. Redekop, M. Luyendijk, A. J. Rijnsburger, J. L. Severens, *PLoS Negl. Trop. Dis.* **2016**, *10*, 1–19.
- [28] S. N. Alam, N. Sharma, L. Kumar, *Graphene*, **2017**, *6*, 1–18.
- [29] X. Yang, X. Jia, X. Ji, *RSC Adv.* **2015**, *5*, 9337–9340.

Submitted: April 8, 2020

Accepted: June 23, 2020